Detection of Envelope Glycoprotein Assembly from Old-World Hantaviruses in the Golgi Apparatus of Living Cells

Petazzi R. A.[1], Koikkarah A. A.[1], Tischler N.D.[2,3], Chiantia S.[1,*]

1. University of Potsdam, Institute of Biochemistry and Biology, Karl-Liebknecht-Str. 24-25, 14476 Potsdam, Germany

2. Fundación Ciencia & Vida, Laboratorio de Virología Molecular, Av. Zañartu 1482, Santiago, Chile

3. Universidad San Sebastián, Santiago, Chile

* E-mail: chiantia@uni-potsdam.de

Abstract

Hantaviruses are emerging pathogens that occasionally cause deadly outbreaks in the human population. While the structure of the viral envelope has been characterized with high precision, the protein-protein interactions leading to the formation of new virions in infected cells are not fully understood yet. In this work, we use quantitative fluorescence microscopy (i.e. Number&Brightness analysis and fluorescence fluctuation spectroscopy) to quantify the interactions that lead to oligomeric spike complex formation in the physiological context of living cells. To this aim, we have analyzed proteins from Puumala and Hantaan orthohantaviruses in several cellular models. For the first time, we quantified the oligomerization state of each protein in relation to its subcellular localization, concentration and the concentration of its interaction partner. Our results indicate that when expressed separately, both glycoproteins can form homo-multimers in a concentration-dependent manner. Fluorescence fluctuation analysis was applied to prove that Gc:Gc contacts observed on virions are also relevant for Gc-Gc interactions in living cells, in the absence of Gn. Furthermore, we proved that the membrane-distal lobes of Gn are not necessary for Gn homo-multimerization. In cells co-expressing both glycoproteins, we observe clear indication of Gn-Gc interactions and the formation of protein complexes with different sizes, while using various labelling schemes to minimize the influence of the fluorescent tags. Our data are compatible with an assembly model according to which hantavirus spikes are formed via the assembly of Gn-Gc hetero-dimers. Furthermore, our results indicate the interconnection of large Gn-Gc hetero-multimers in the Golgi apparatus. Such large glycoprotein multimers may be identified as multiple interacting viral spikes and provide a possible first evidence for the initial assembly steps of the viral envelope, within this organelle, directly in living cells.

Introduction

36
37 Hantaviruses (HV) are single-stranded, negative sense RNA viruses belonging to the
38 *Hantaviridae* family of the order Bunyavirales. While usually infecting rodents, insectivorous
39 mammals or bats (1), these emerging pathogens can occasionally cause deadly outbreaks in the
40 human population (2). Their segmented genome encodes at least a nucleocapsid protein, a
41 RNA-dependent RNA polymerase and a glycoprotein precursor (GPC) (3). The assembly of
42 HV particles in infected cells is a complex process that relies on the precise spatial and temporal
43 organization of several viral proteins. The specific molecular mechanisms driving protein-
44 protein interactions in this context are not fully characterized yet.

45 While negative-stranded RNA viruses typically assemble and bud at the plasma membrane (4,
46 5), Bunyavirales are mostly characterized by intracellular maturation (6). In all HVs, two
47 glycoproteins (GPs) form surface spikes and are derived from the GPC encoded in the M
48 segment of the tripartite genome. After, The N-terminal Gn and C-terminal Gc have been
49 suggested to be cleaved co-translational by cellular signal peptidases (7). The interplay between
50 Gn and Gc has a fundamental importance in HV assembly and budding (8, 9).

51 Early studies that aimed to localize singularly expressed Gn and Gc showed variations for
52 different members of the Bunyavirales order (10, 11). However, co-expression of both HV GPs
53 results, in general, in their translocation to the Golgi apparatus (GA) (12-16). This holds true
54 also for recombinant proteins that are not derived from a common precursor (17).

55 On the other hand, not much is known about where and how Gn-Gc hetero-complexes are
56 initially assembled in an infected cell. It is therefore of great interest to address the role of
57 protein-protein interactions involved in the maturation of the HV spike complex. Cryo-EM
58 studies on the surface of Tula virus (TULV) indicated that such a complex is formed by square-
59 shaped Gn-Gc hetero-octamers composed of four Gn and Gc molecules (18, 19). The presence
60 of Gn-Gc heteromultimers has also been confirmed by biochemical assays of virion extracts
61 (20). The fitting of the Gn ectodomain crystal structure of PUUV into the spike density of a
62 cryo-EM tomography reconstruction of TULV revealed that Gn forms the membrane distal
63 tetrameric lobes with Gc occupying the volume underneath (21). The design of cysteine
64 mutations at the two-fold axis of a crystallographic Gc dimer (22) further proved that Gc:Gc
65 contacts connect adjacent spikes and additional residue substitutions showed that the
66 interactions at the inter-spike Gc:Gc interface are crucial for virus particle assembly (23).

67 A quantitative assessment of Gn-Gc interactions leading to the formation of spike complexes
68 in a more physiological environment within a living cell is still lacking. According to the model

2

69   proposed by Hepojoki *et al.* (24), the assembly of HV spikes might follow two pathways. In

70   one case (referred to as "assembly model 1" in what follows), homotypic interactions between

71   Gn monomers lead first to the formation of a tetrameric core to which Gc proteins subsequently

72   bind to form larger hetero-complexes. In the second case (i.e. "assembly model 2"), the

73   formation of a Gn-Gc heterodimer is the first step in the formation of the final spike complex

74   (via interactions between four Gn-Gc heterodimers).

75   While the above-mentioned biochemical and structural characterizations of virion surface

76   provide information about completely formed spike complexes, alternative approaches are

77   needed to clarify how protein-protein interactions occur in different intra-cellular

78   compartments, leading to the spike and inter-spike assembly.

79   Here, we apply Number and Brightness (N&B) analysis to quantify the homo- and hetero-

80   oligomerization of HV Gn and Gc, directly in living cells. Previously, we have used this method

81   to demonstrate that Gn possesses a significantly higher tendency to oligomerize, compared to

82   Gc. This approach was based on the bulk analysis of several cells, in a restricted protein

83   concentration range, and required some assumptions on the actual presence of specific

84   multimeric states (e.g. Gn tetramers) (16).

85   In this new work, we provide a complete quantitative characterization of HV GPs homo-

86   multimerization, over a large concentration range, for two different virus strains and in different

87   cell models. Also, we investigate the hetero-interactions between Gn and Gc using a novel

88   quantitative fluorescence assay based on bidirectional expression vectors, allowing us to

89   monitor the oligomerization of one protein as a function of the concentration of the other.

90   Finally, we determine the most probable of the proposed assembly models and provide the first

91   experimental evidence of HV assembly directly in the GA of living cells.

Materials and Methods

Cloning and generation of chimeric proteins

Unless otherwise specified, glycoprotein gene sequences refer to the PUUV strain. Original plasmids of signal peptide (SP)-mEYFP-Gn and SP-mEYFP-Gc were previously described (16). Plasmids encoding Gn and Gc preceded by three HA tags (HAtag-Gn, HAtag-Gc) were a gift from A. Herrmann (Humboldt Universität zu Berlin). A monomeric variant of EGFP, containing the A206K mutation (25), was PCR amplified from a mEGFP-C1 vector and cloned into these vectors to substitute mEYFP and generate SP-mEGFP-Gn and SP-mEGFP-Gc respectively. Vectors for the expression of N-terminally mEGFP-tagged Gn and Gc mutants were synthesized by Twist Bioscience (San Francisco, CA, USA): a Gn variant comprising of amino acids 387-658 and lacking part of the ectodomain (ΔGn) and Gc variants with point mutations at the Gc:Gc interface (H303C Gc, H303E Gc). ΔGn contains a flexible linker between mEGFP and the truncated Gn (EGKSSGSGSESKST) (26, 27). A plasmid for bi-directional expression was a gift from K. Arndt (Universität Potsdam). Promoters TTC31 and CCDC142 allowed simultaneous expression of encoded genes (28). mEGFP and mCherry2 were PCR-amplified and cloned into the two expression cassettes flanked by restriction sites BamHI/EcoRI and SacI/KpnI respectively, to obtain mEGFP←→mCherry2. A construct with mCherry2 and mEGFP cloned into SacI/KpnI and BamHI/EcoRI restriction sites, respectively, was also produced (mCherry2←→mEGFP). Unlabeled GP sequence (SP-Gn and SP-Gc) were PCR-amplified and separately cloned into the BamHI/EcoRI cassette to produce SP-Gn←→mCherry2 and SP-Gc←→mCherry2. A plasmid encoding the whole Hantaan virus (HTNV) GPC was a gift from Dr. S. Weiss (Charité, Berlin). The signal peptide was introduced at the N-terminus of mEGFP-C1 and Gn and Gc were independently amplified and cloned into this vector to obtain HTNV SP-mEGFP-Gn and SP-mEGFP-Gc. Golgi-mTurquoise was a gift from Dorus Gadella (Addgene plasmid # 36205) and has been described before (16). ER-mCherry, Golgi-mCherry and MyrPalm-mEGFP were previously described in (16). ER-mEGFP and Golgi-mEGFP were obtained by PCR amplification of mEGFP from mEGFP-C1 and subtitution of the FP via digestion/ligation at the restriction sites AgeI/BsrgI. FastDigest enzymes (Thermo Scientific, Waltham, MA, USA) were used for all restriction reactions. Ligations were performed with T4 DNA Ligase (Thermo Scientific) at 16° overnight. All cloning were tested by Sanger sequencing of expression plasmids.

Cell culture and transfection

Chinese hamster ovary cells (CHO-K1), adenocarcinomic human alveolar basal epithelial cells (A549), human embryo kidney cells (HEK-293T) and VeroE6 cells were maintained in Dulbecco's modified Eagle's medium containing 10% fetal bovine serum, 100 U/mL penicillin, 0.1 mg/mL streptomycin and 4 mM L-Glutamine. Cells were passaged every 3–5 days, no more than 15 times. All solutions, buffers and media used for cell culture were purchased from PAN-Biotech (Aidenbach, Germany). $3\text{-}6 \cdot 10^5$ cells were plated on glass-bottom 35-mm-diameter plates (CellVis, Mountain View, CA or MatTek Corp., Ashland, MA) 48 hours before experiments. Fusion protein expression plasmids were transfected into (70-90% confluent) cells using Turbofect™ (Thermo Scientific) according to the manufacturer's protocol, 20-24 hours prior to experiments. VeroE6 cells were transfected with Lipofectamine™ 3000 (Thermo Scientific) instead, since they are not susceptible to transfection by Turbofect™.

Confocal fluorescence microscopy

Confocal fluorescence images were obtained with a 40× water immersion objective (NA 1.2) at 21°C on a Zeiss LSM780 (Carl Zeiss, Oberkochen, Germany) confocal microscope with a frame size of 512 x 512 pixels. mTurquoise was excited at 405 nm using a laser diode and observed in 475–490 nm detection range. mEGFP was excited at 488 nm using a CW Argon laser (Lasos, Jena, Germany) and detected in the range of 498–606 nm. mCherry2 was excited at 561 nm using a laser diode and observed in 578-695 nm detection range. Images with more than one fluorescent species were recorded sequentially to minimize signal cross-talk.

For intracellular immunofluorescence staining, cells were washed three times with phosphate-buffered saline with calcium and magnesium (PBS, PAN-Biotech) and fixed with 3.7% paraformaldehyde (Sigma-Aldrich, Munich, Germany) for 25 min at room temperature. Afterwards, the cells were washed three times with PBS before permeabilization with 0.2% Triton X-100 (Sigma-Aldrich) and 0.2% bovine serum albumin (PAN-Biotech) for 20 min. After three more washing steps, cells were incubated with anti-HAtag rabbit primary antibody (Abcam, Berlin, Germany, ab13511) for 1 h. This procedure was repeated for the Alexa488-conjugated secondary antibody (goat anti rabbit IgG, Thermo Scientific) and the immunostaining was concluded with three washing steps.

5

156 **Fluorescence Correlation Spectroscopy**

157 Point FCS measurements (29) were performed for 120 s on a Zeiss LSM780 microscope and

158 recorded using the Zen Black software. mCherry2 was excited at 561 nm using a laser diode

159 and observed in 578-695 nm detection range. Laser powers were adjusted to keep

160 photobleaching below 20%. Typical values were ~6 µW (561 nm). The size of the confocal

161 pinhole was set to 1 airy unit. Intensity time series were analyzed with the Zen software to

162 obtain the auto-correlation function (ACF):

163
$$G(\tau) = \frac{\langle \delta F(t) \delta F(t + \tau) \rangle}{\langle F(t) \rangle^2}$$

164

165 where $\delta F(t) = F(t) - \langle F(t) \rangle$. The ACF was fitted as described in (30). The inverse of the

166 amplitude G(0) indicates the number of particles in the effective confocal volume (29). To

167 calibrate the confocal volume, pFCS measurements with Alexa Fluor® 488 or Rhodamine B

168 dissolved in water at 50 nM were performed at the same laser power. The structure parameter

169 S (defined as the ratio between the vertical and lateral dimension of the theoretical confocal

170 ellipsoid) was fixed to the value determined in the calibration measurement (typically around 4

171 to 8).

172

173 **Number and Brightness**

174 Number and Brightness analysis (N&B) was performed as previously described (16, 31).

175 Briefly, $3\text{-}6 \cdot 10^5$ cells were plated onto 35 mm glass-bottom dishes (CellVis, Mountain View,

176 CA or MatTek Corp., Ashland, MA) 48 h prior to the experiment and transfected as described

177 above. Confocal images were acquired using a Zeiss LSM780 microscope. The 488 nm

178 excitation from a CW Argon laser was focused with a 40× UPLS Apochromat 1.2 NA water

179 objective into the sample. The fluorescence signal was collected by a Zeiss QUASAR

180 multichannel GaAsP detector in a 498-606 nm range in photon counting mode. The laser power

181 was set so that the photon count rate and bleaching remained below 1 MHz and ca. 20%,

182 respectively (i.e. typical laser power values were ≤ 4 µW). Images of 128 × 128 pixels were

183 acquired with pixel dimensions ~ 400 nm and a pixel dwell time of 25-50 µs. Image time-stacks

184 of 105 scans were collected using the Zeiss Black ZEN software. The intensity time-stacks data

185 were analyzed using a self-written Matlab code (The MathWorks, Natick, MA, USA). The

186 Matlab algorithm implements the equations from Digman *et al.* (32) for the specific case of

6

187   photon-counting detectors, thus obtaining the molecular brightness and number as a function

188   of pixel position. Regions of interest (e.g. ER, GA) were selected in cell images by applying a

189   mask obtained from the intensity map of co-transfected ER-mCherry2 or Golgi-mCherry2.

190   To correct for photobleaching effects and minor cell movements, a boxcar-filter pixel-wise with

191   8-frames length was used, as previously described (16, 33). Saturation of detectors leading to

192   artefactual reduction in brightness was avoided by excluding pixels in which photon-counting

193   rates exceeded ~ 1 MHz. Using this selection criterion, saturation induced brightness decrease

194   was kept below 10 %. To further correct the detector response, we took into account the signal

195   originating from a thin film containing immobilized fluorophores (31) .

196   Finally the brightness values obtained from every single measurement were normalized to

197   account for the monomer brightness ε_m and the fluorescence probability (p_m), which

198   determines the detectability of the tag (30). Briefly, the absolute brightness ε_i was compared to

199   the brightness of the monomer and corrected using previously determined values for p_m, thus

200   obtaining an estimation of the multimerization state:

201

$$\varepsilon_n = \frac{1}{p_m}\left(\frac{\varepsilon_i}{\varepsilon_m} - 1\right) + 1.$$

202   HV GPs are mostly found in the ER and GA (13, 14, 16, 34). Therefore, ε_m was determined for

203   standard fluorescent proteins localized in the same subcellular compartments: ER-mEGFP (to

204   be compared to Gn) and Golgi-mEGFP (to be compared to Gc). The actual multimeric state of

205   these specific reference constructs was never quantified before. For this reason, the

206   corresponding monomeric molecular brightness reference values were obtained by subjecting

207   the specimen to several bleaching cycles (10-20s at a laser power 5-10 times higher than the

208   measuring parameters) followed by N&B data acquisition. Since completely bleached

209   multimers do not contribute to the overall brightness value, the lowest constant brightness

210   measurement obtained indicates indeed the monomer reference brightness value (Fig. S1). We

211   found that ER-mEGFP and Golgi-mEGFP form multimers (containing ca. 3-6 units) and that

212   the monomeric brightness reference value can be calculated in a reproducible manner after the

213   step-wise bleaching procedure (~1 kHz/molecule). Furthermore, we observed that the monomer

214   brightness values for the ER and GA markers were comparable to that of a membrane-

215   associated monomeric fluorescent construct (i.e. MyrPalm-mEGFP) that is typically used in

216   quantitative fluorescence microscopy experiments (16, 35). For this reason, we proceeded to

217   use MyrPalm-mEGFP as reference for further measurements, thus avoiding the time-

218   consuming step-wise bleaching calibration process.

219 The concentration N (in monomer units) was calculated by dividing the mean count rate in the
220 ROI by the absolute brightness of the reference monomer:

221
$$N = \frac{\langle F(t) \rangle}{\varepsilon_m}$$

222 This corresponds to the number of monomers observed in the confocal volume (see previous
223 paragraph). This number was then converted in concentration (i.e. monomers/μm^3) using a
224 value of 0.25 µm for the lateral size of the confocal volume. The structure parameter S of the
225 confocal volume was the value determined in the calibration measurement, typically around 4
226 to 8. When plotting brightness vs. concentration data, segmented averages were calculated by
227 dividing the whole concentration range in bins of variable width (containing ca. 1-4 points) and
228 calculating mean values therein. Bins contained in general fewer points for high concentration
229 values, i.e. in regions where the density of data points was lower. Unless differently stated, an
230 empiric model was fitted to the data:

231

232
$$\varepsilon = 1 + \frac{a}{1 + e^{-k\,(Concentration - C_{1/2})}}$$

233 where ε is the normalized brightness and *a, k* and $C_{1/2}$ are fitting parameters. $C_{1/2}$ in particular
234 is an indicator of the concentration at which half of the total protein is monomeric, in the simple
235 approximation that only two oligomeric species are present (e.g. a mixture of 10 tetramers and
236 40 monomers).

237 Finally, in the case of mixtures of two different oligomeric states, the corresponding molar
238 fractions n_1 and n_2 were determined by inverting the following equation:

239
$$\varepsilon = \frac{\varepsilon_1^2 \cdot n_1 + \varepsilon_2^2 \cdot n_2}{\varepsilon_1 \cdot n_1 + \varepsilon_2 \cdot n_2}$$

240 where ε_i indicates the multimerization of the i-th species and ε is the observed normalized
241 brightness.

Results

243

Gn forms homo-tetramers in a concentration-dependent manner

In order to dissect the process of spike formation from GP monomers, we independently quantified the concentration-dependent multimerization of either Gn or Gc, at different protein concentrations, directly in living cells (36, 37). While local protein concentration cannot be actively controlled, it is possible to collect data from several cells randomly expressing different protein amounts. In order to quantify Gn (or Gc) multimerization, we performed N&B analysis. N&B is a fluorescence fluctuation-based method that allows to calculate the concentration and the molecular brightness of diffusing fluorescent molecules (32). The latter parameter indicates the amount of fluorescence signal detected for a single independent fluorescent molecular complex (e.g. a single protein tetramer) in the unit of time. The molecular brightness increases therefore if several monomers diffuse together (i.e. as a single entity) through the observation volume. By normalizing the measured value by the molecular brightness of a monomeric reference, it is possible to calculate the amount of fluorophores in the complex and, thus, its multimerization state (16, 30).

We analyzed mEGFP-tagged fluorescent constructs derived from two HV strains GPs in different cell line models (i.e. CHO-K1, HEK-293T, A549 and Vero E6 cells). In particular, the alveolar epithelial cells A549 were selected since "New World" HV strains can cause respiratory diseases (Hantavirus Pulmonary syndrome, HPS). Vero E6 cells are often used for the propagation and isolation of HVs. N-terminal labelling with mEGFP was preferred to C-terminal labelling based on previous results indicating the importance of GP C-terminus in protein localization (16). ER and GA markers – mCherry fusion proteins (FPs) bound to the respective retention peptides – were used to identify regions of interest (ROIs) and restrict the N&B analysis to specific cellular compartments.

In the case of PUUV GPs, SP-mEGFP-Gn was retained in the ER, while SP-mEGFP-Gc significantly partitioned in the GA (Fig. 1 A and C), as expected from previous studies (16) and controls with unlabeled GPs (Fig. S2). According to N&B analysis (Fig. 1 B), SP-mEGFP-Gn consistently showed a concentration-dependent oligomerization behavior, ranging from monomers to tetramers. Of interest, the measured brightness did not significantly exceed the values expected for tetramers, even at the highest observable concentrations.

273

274
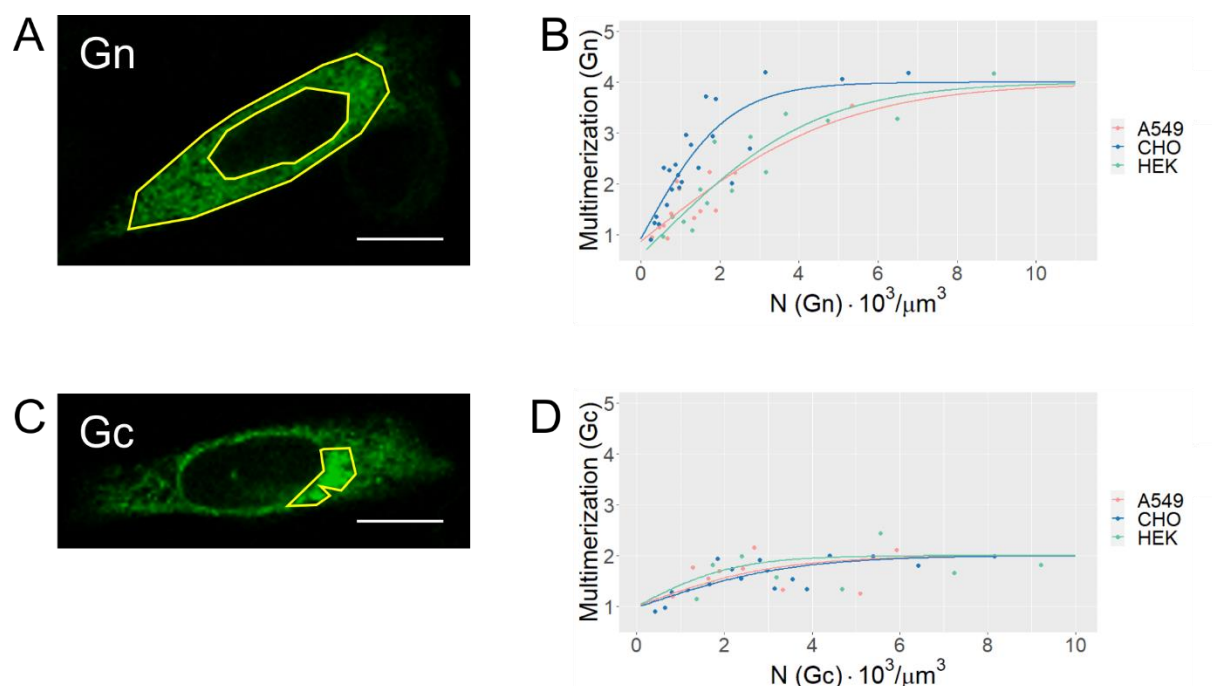
275 **Figure 1: Concentration-dependent multimerization of PUUV Gc and Gn.** Different cell lines expressed either
276 SP-mEGFP-Gn (A, B) or SP-mEGFP-Gc (C, D). A, C) Representative fluorescence intensity maps of mEGFP-
277 tagged GPs in CHO cells. Intensity maps of single cells were obtained as an average of 105 frames (128×128
278 pixels) collected over $\sim$2–3 min with a pixel dwell time of 25-50 µs. Examples or ROIs used for multimerization
279 analysis are shown in yellow. White bars are 5 µm. B,D) Protein multimerization as a function of total protein
280 concentration (in monomer units). N&B analysis was applied to a ROI in each cell (ER for Gn, Golgi for Gc)
281 identified by an ER-mCherry or Golgi-mCherry marker. Multimerization values were obtained from molecular
282 brightness normalization, as described in the Materials and Methods section. Each point is calculated from the
283 average brightness extracted from ROIs in 2-4 cells with similar protein concentrations. Solid lines are a fit of an
284 empirical model (see Materials and Methods) and are meant as guide to the eye. Each dataset is obtained from at
285 least 5 independent experiments, for a total of approx. 50-70 examined cells.

286

287 The $C_{1/2}$ concentration values (defined as the concentration at which half of the total protein is

288 monomeric, in the simple approximation that only monomers and tetramers are present) range

289 between $\sim$1$\cdot$10^3 (CHO) and $\sim$3$\cdot$10^3 (A549, HEK) monomers/µm³, for different cell lines.

290 On the other hand, SP-mEGFP-Gc multimerization only slightly correlates with its

291 concentration in the GA (Fig. 1 D) or in the ER (Fig. S3). More in detail, SP-mEGFP-Gc

292 oligomerization values ranged between those of monomers and dimers and did not exceed the

293 value expected for dimers, even at the highest observable concentrations.

294 Analogous measurements were performed additionally in Vero E6 cells: although the

295 expression of SP-mEGFP-Gn never reached concentrations high enough to observe a strong

296 difference with SP-mEGFP-Gc or the clear formation of tetramers (Fig. S4, possibly due to

297 sub-optimal transfection efficiency), GP multimerization might be compatible with that

298 observed in other cell lines, at least at those low protein concentrations.

10

299   In order to assess whether HV GPs multimerization varies among different strains, Hantaan

300   virus (HTNV) SP-mEGFP-Gn and SP-mEGFP-Gc were observed in CHO-K1 cells. Differently

301   from PUUV GPs, both separately expressed proteins localize preferentially in the ER (Fig. 2 A

302   and B). The quantification of the multimerization state via N&B analysis shown in Fig. 2 C

303   indicates that SP-mEGFP-Gn forms monomers at low concentrations and tetramers at higher

304   concentrations, similar to PUUV proteins. Also HTNV SP-mEGFP-Gc behaves similarly to its

305   PUUV counterpart, displaying a multimerization state between monomers and dimers, over the

306   explored concentration range.

307

308
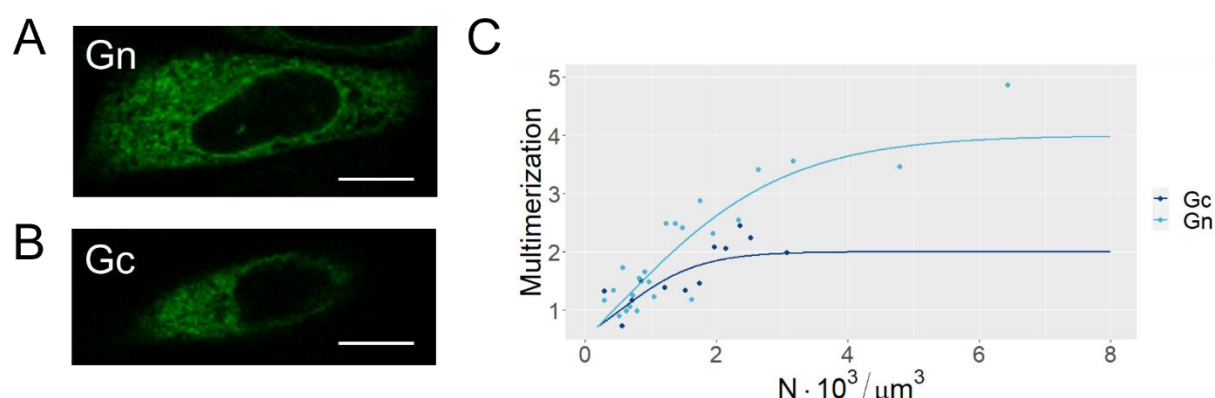
309   **Figure 2: Concentration-dependent oligomerization of HTNV Gc and Gn.** CHO-K1 cells were transfected
310   with HTNV SP-mEGFP-Gn and SP-mEGFP-Gc vectors, respectively. A, B) Representative fluorescence intensity
311   maps of mEGFP-tagged GPs in CHO cells. Intensity maps of single cells were obtained as an average of 100
312   frames (128×128 pixels) collected over $\sim$2–3 min with a pixel dwell time of 25-50 μs. White bars are 5 μm. C)
313   Protein multimerization as a function of total protein concentration (in monomer units). N&B analysis was applied
314   to a ROI in each cell identified by an ER-mCherry marker. Multimerization values were obtained from molecular
315   brightness normalization, as described in the Materials and Methods section. Each point is calculated from the
316   average brightness extracted from ROIs in 2-4 cells with similar protein concentrations. Solid lines are a fit to an
317   empirical model (see Materials and Methods) and are meant as guide to the eye. Each dataset is obtained from at
318   least 5 independent experiments, for a total of ca. 40-60 examined cells.

319

320   Altogether, these results indicate that, irrespective of specific cell line model or HV strain

321   investigated, Gn can form oligomers (up to tetramers) when singularly expressed in cells. Gc,

322   on the other hand, is found in monomeric and dimeric states at all investigated concentration

323   levels.

324

325

326

327 **Gc:Gc interactions observed on the viral surface occur in cells also in the absence of Gn-**
328 **Gc complexes**

329 The Gc:Gc inter-spike contact region has been previously investigated by structure-guided
330 biochemical assays of Andes HV-like particles to determine which residues are involved in
331 stabilizing the interaction (23). In particular, cysteine substitutions of selected residues at the
332 Gc:Gc interface showed a higher stability of Gn-Gc hetero-multimers. The introduction of
333 repulsive interactions by residues with the same charge at the Gc:Gc interface, instead, led to a
334 decrease in protein-protein interactions. Since the Gc:Gc interface region is highly conserved
335 among different HV strains (23), we analyzed the same mutants (i.e., H303C and H303E) for
336 the mEGFP-tagged PUUV Gc construct. The aim of this experiment was to verify whether
337 Gc:Gc contacts relevant for inter-spike interactions play also a role in determining interactions
338 between Gc monomers in living cells.

339 Expression in of Gc mutants in CHO-K1 cells indicated that both constructs are homogeneously
340 distributed in the ER (Fig. 3, A and B) but were expressed with significantly different
341 efficiencies (data not shown). We then selected a shared concentration range (i.e. $1\text{-}5\cdot10^3$
342 monomers / μm^3) for the three Gc constructs – wild type and the two mutants – and compared
343 protein multimerization for these samples. Fig. 3 C shows that, compared to wt Gc, the H303E
344 mutant displays a significantly lower multimerization. In the approximation that only Gc
345 monomeric and dimeric assemblies are present (as suggested by the results reported in the
346 previous paragraph), the observed average multimerization values correspond to a mixture of
347 ca. 4:1 monomers:dimers for this mutant (cfr. approx. 3:2 monomers:dimers for the wt). On the
348 other hand, H303C Gc mutants appear to be present almost exclusively in dimeric form, as
349 expected from previous *in vitro* investigations of virus-like particles (23).

350

12

351
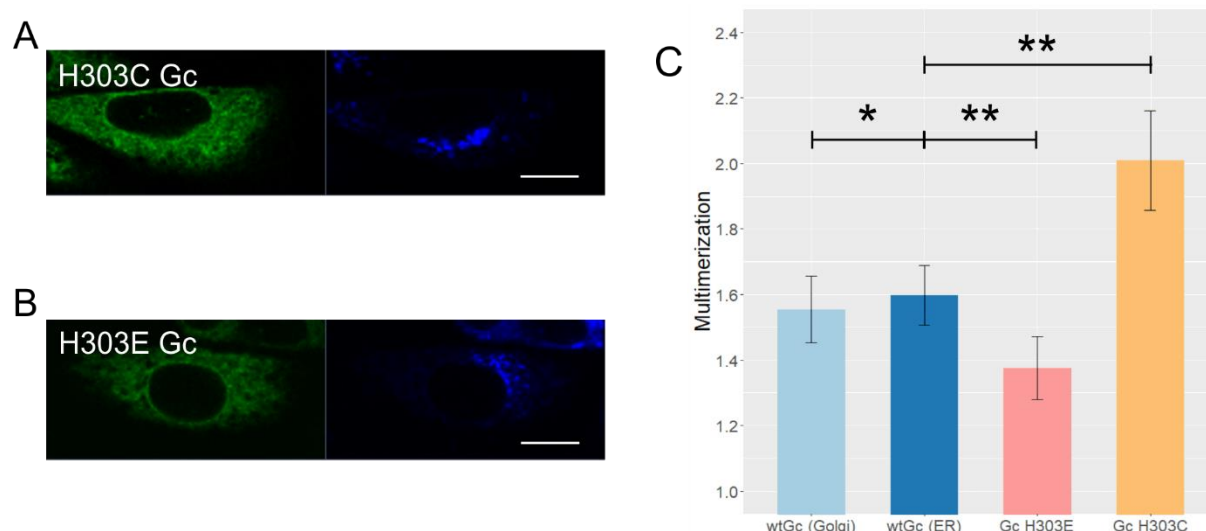
Figure 3 Brightness analysis of PUUV Gc mutants. CHO-K1 cells were transfected with SP-mEGFP-Gc(H303C), SP-mEGFP-Gc(H303E) or SP-mEGFP-Gc (wt) vectors. A, B) Representative fluorescence intensity images of PUUV Gc mutants H303C and H303E (left panels, in green) and Golgi-mTurquoise marker (right panels, in blue) co-expressed in CHO-K1 cells. Intensity images were obtained as an average of 105 frames (128 × 128 pixels) collected over ~2–3 min with a pixel dwell time of 25-50 μs. White bars are 5 μm. C) Normalized multimerization values calculated via N&B analysis. In order to compare all the different constructs displaying varying expression efficiencies, multimerization values were selected in the shared range of $1\text{-}5 \cdot 10^3$ monomers / μm³. Bars indicate the median of at least 3 separate experiments and ca. 30 cells, error bars are calculated as the standard error of the mean. T-test significance is represented by asterisks: $p > 0.5$ (*), $p < 0.05$ (**).

361

362 These results indicate that Gc:Gc dimerization in our cellular model occurs through the same

363 contacts, as on the viral surface between spikes. Also, N&B analysis can be successfully applied

364 to detect subtle changes in Gc-Gc interactions (e.g. induced by point mutations) and such

365 interactions do not appear to be significantly hindered by the presence of a fluorescent tag.

366

The membrane-distal lobes of PUUV Gn are not necessary for tetramer formation

368 Based on the structural characterization of HV spikes, the central stalk of the Gn ectodomain

369 (aa 388 to 484), Gn transmembrane region and endodomain may be responsible for homo-

370 oligomerization (15, 21). Based on this criteria, we designed a Gn mutant lacking the membrane

371 distal lobes of the ectodomain (21), thus obtaining SP-mEGFP-linker-Gn(387-658) (ΔGn).

372 Protein localization was not influenced by the lack of the Gn lobes and the protein was still

373 retained in the ER, similarly to wt SP-mEGFP-Gn (data not shown). As shown in Fig. 4,

374 quantification of protein multimerization via N&B analysis indicates that ΔGn forms tetramers

375 at high concentrations. The $C_{1/2}$ value (ca. 5000 monomers / μm³) is significantly higher than

376 the one observed for wt SP-mEGFP-Gn (ca. 1500 monomers / μm³, see Fig. 1 B and 4),

13

377 implicating that tetramerization is favored in the case of the wt protein, although the Gn lobes

378 are not strictly required.

379

380

381
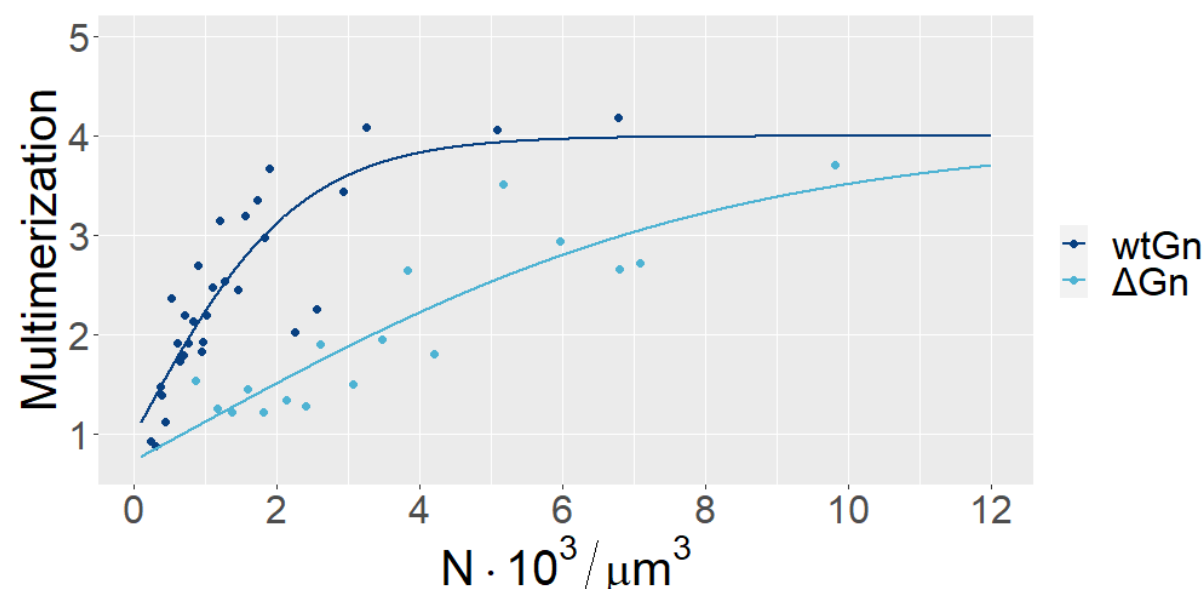
Figure 4: Comparative brightness analysis of PUUV Gn wt and ΔGn. CHO-K1 cells expressing ΔGn were analyzed. The mutant comprises amino acids 387-635 and is lacking part of the ectodomain. The graph shows protein multimerization as a function of total protein concentration (in monomer units), obtained via N&B analysis as described in the Materials and Methods section. The results for SP-mEGFP-Gn (wtGn) are shown as comparison. Each point is calculated from the average brightness extracted from ROIs in 2-4 cells with similar protein concentrations. Solid lines are a fit to an empirical model (see Materials and Methods) and are meant as guide to the eye. Each dataset is obtained from at least 5 independent experiments, for a total of ca. 50 examined cells.

390

PUUV Gn forms high-order oligomers in the Golgi apparatus in the presence of Gc: 1) using fluorescent and untagged Gc constructs

393 We proceeded to study the interaction between Gn and Gc by co-expressing the two GPs in

394 CHO-K1 cells and measuring their multimerization state via N&B analysis (Fig. 5). Co-

395 expression of SP-mEGFP-Gn and SP-mCherry2-Gc caused an enrichment of both proteins to

396 the GA, as previously observed (see Fig. S5 and (16)). The fluorescence signal (i.e. the protein

397 concentration) in the ER was too low to obtain reproducible brightness values and, therefore,

398 we quantified the multimerization of SP-mEGFP-Gn in the GA. Interestingly, Gn does not

399 appear to form tetrameric assemblies (cfr. the case of SP-mEGFP-Gn in the absence of Gc, Fig.

400 1), even at relatively high concentrations (Fig. 5 E). This might be caused by the steric hindrance

401 of FPs fused to the N-terminal of both GPs. In order to minimize this effect, we analyzed Gn

14

402   multimerization also in cells co-expressing SP-mEGFP-Gn and unlabeled SP-Gc. While Gc is

403   not detectable via fluorescence microscopy, we inferred its presence by the localization pattern

404   of SP-mEGFP-Gn and limited the analysis to those cells with a clear partitioning of Gn in the

405   GA. In these cases, SP-mEGFP-Gn was consistently found in higher-order multimers, up to

406   octamers in average (Fig. S6).

407

408   PUUV Gn forms high-order oligomers in the Golgi apparatus in the presence of Gc:

409   2) using bi-directional GP constructs

410   Transfecting cells with SP-mEGFP-Gn and an unlabeled SP-Gc construct allows an

411   approximate characterization of Gn-Gc interactions. Although we focused on Gn localization

412   in the GA as clue of the presence of Gc, this approach does not allow to confirm that both

413   fluorescent Gn and unlabeled Gc are indeed present in every examined cell. We therefore

414   adopted a novel alternative strategy that, additionally to solving the above-mentioned problem,

415   allowed us to estimate the amount of unlabeled Gc. We transfected CHO-K1 cells with a vector

416   for the expression of SP-mEGFP-Gn and, separately, a bi-directional vector for the concurrent

417   expression of SP-Gc and cytosolic mCherry2 (indicated as SP-Gc$\leftrightarrow$mCherry2) (Fig. 5A-D).

418   The measured concentration of mCherry2 can be then used to estimate the amount of unlabeled

419   SP-Gc in the GA (Fig. S7). The concentration of SP-mEGFP-Gn outside the GA was too low

420   to detect significant and reproducible protein multimerization. On the other hand, the

421   quantification of SP-mEGFP-Gn oligomeric state as function of its concentration in the GA

422   confirmed our initial estimations, showing higher average oligomerization states ranging up to

423   roughly dodecamers (Fig. 5 E), far above the typical values observed for of SP-mEGFP-Gn in

424   the absence of Gc. Of note, since the multimerization values do not reach a constant value at

425   high concentrations, it must be assumed that of SP-mEGFP-Gn is, in general, present as a

426   mixture of different multimeric species. In this case, N&B analysis provides simply a weighted

427   average value for the multimerization state. Finally, we observed that SP-mEGFP-Gn

428   multimerization state has only a weak correlation to the concentration of unlabeled SP-Gc (Fig.

429   S8).

430

15

431

432
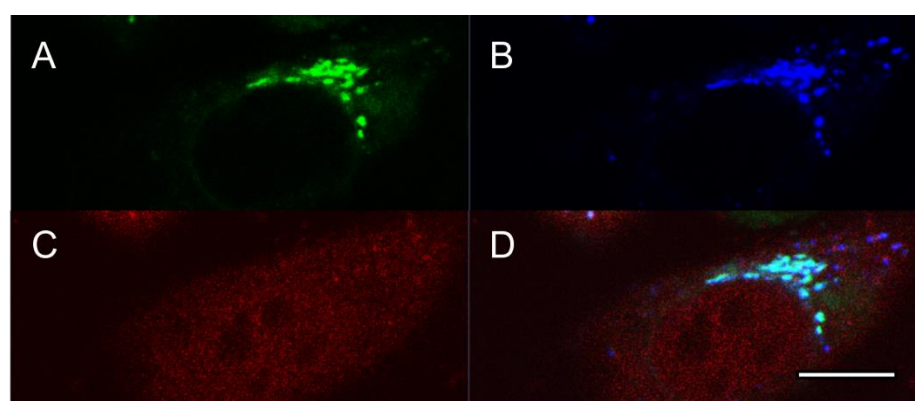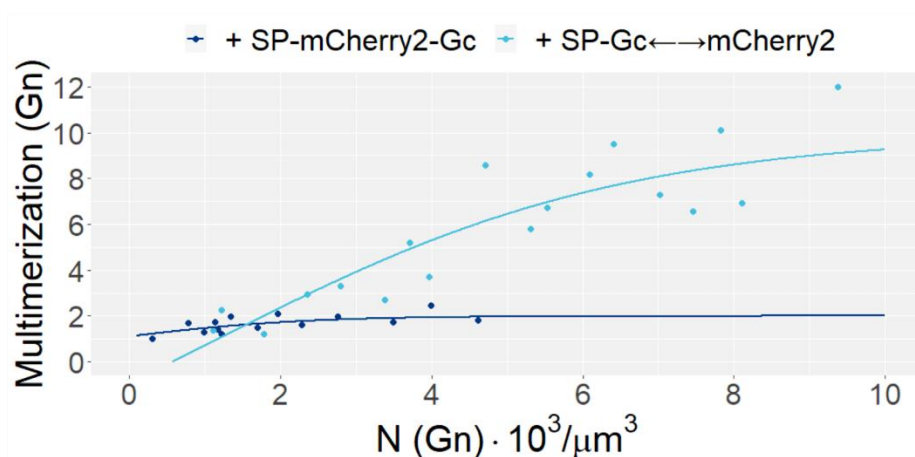
Figure 5: Concentration-dependent oligomerization of PUUV Gn in the presence of Gc. CHO-K1 cells expressed SP-mEGFP-Gn and either SP-mCherry2-Gc or SP-Gc (together with cytosolic mCherry2 within a bi-directional vector; indicated as SP-Gc←→mCherry2). A-D) Representative confocal microscopy image of CHO-K1 transfected with SP-mEGFP-Gn and SP-Gc←→mCherry2] vectors. Split view of SP-mEGFP-Gn (A), mGolgi-Turq marker (B), cytosolic mCherry2 (C) and merged channels (D). White bars are 5 μm. E) SP-mEGFP-Gn multimerization as a function of its total concentration (in monomer units), obtained via N&B analysis as described in the Materials and Methods section. The analysis was restricted to cells which showed significant expression of mCherry2. Each point is calculated from the average brightness extracted from ROIs in 2-3 cells with similar protein concentrations. Solid lines are a fit to an empirical model (see Materials and Methods) and are meant as guide to the eye. Each dataset is obtained from at least 4 separate experiments, for a total of ca. 40 cells.

443

PUUV Gc increases its multimerization in the GA in the presence of Gn

We proceeded to investigate the multimerization behavior of SP-mEGFP-Gc in the presence of SP-Gn←→mCherry2 (i.e. a non-labelled SP-Gn construct concurrently expressed with cytosolic mCherry2). While the intra-cellular localization of SP-mEGFP-Gc in the GA is not altered by the presence of the other GP (Fig. 6 A-D), its molecular brightness is significantly higher than that measured in the absence of Gn, with values ranging between two and four (Fig.

450 6 E). The apparent multimerization behavior of SP-mEGFP-Gc seems to be only weakly

451 correlated to either its concentration (Fig. 6 E) or to SP-Gn concentration (Fig. S9).

452

453
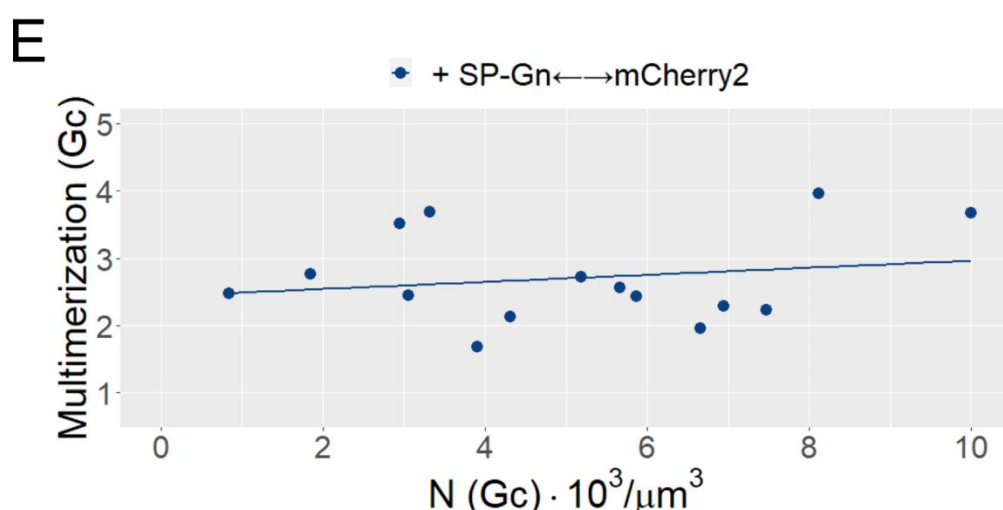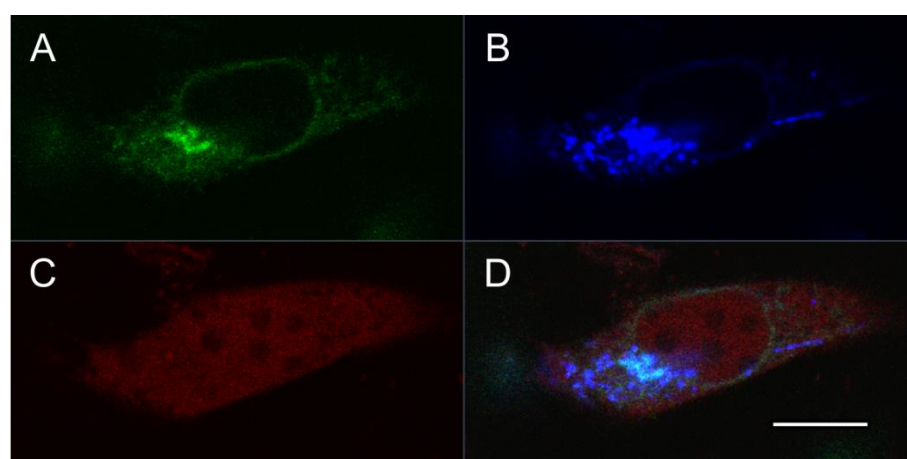
Figure 6: Concentration-dependent oligomerization of PUUV Gc in the presence of Gn. CHO-K1 cells expressed SP-mEGFP-Gc and SP-Gn (together with cytosolic mCherry2 within a bi-directional vector; indicated as SP-Gn←→mCherry2). A-D) Representative confocal microscopy image of CHO-K1 transfected with SP-mEGFP-Gc and SP-Gn←→mCherry2 vectors. Split view of SP-mEGFP-Gc (A), Golgi-mTurquoise marker (B), cytosolic mCherry2 (C) and merged channels (D). White bars are 5 μm. B) SP-mEGFP-Gc multimerization as a function of total Gc concentration (in monomer units), obtained via N&B analysis as described in the Materials and Methods section. The analysis was restricted to cells which showed significant expression of mCherry2. Each point is calculated from the average brightness extracted from ROIs in 2-3 cells with similar protein concentrations. Solid lines are a fit to an empirical model (see Materials and Methods) and are meant as guide to the eye. Each dataset is obtained from at least 4 separate experiments, for a total of ca. 35 cells.

466

467

468

17

469

Discussion

470   The formation of homo- and hetero-complexes between Gn and Gc proteins is supposed to drive

471

472   the assembly of new virions in infected cells. In spite of the importance of these inter-molecular

473   interactions, there is a general lack of information regarding the oligomeric state of HV GPs

474   directly during the process of virus assembly. In this study, we addressed this question and

475   quantified the interactions that lead to oligomeric spike complex formation in the physiological

476   context of living cells.

Limited Gn and Gc homotypic-interactions

477

478   In the case of Gc singularly expressed in different cell lines, the protein was found in monomeric

479   and dimeric form both in the ER and GA (Fig. 1 D, 3 C, S3, S4). On the other hand, Gn

480   oligomers ranged in size between monomers and tetramers, with a considerable correlation to

481   the local protein concentration in the ER (Fig. 1 B). These results validate the hypothesis that

482   HV spike formation is modulated by local protein concentration (8). Also, the formation of Gn

483   tetramers and dimeric Gc:Gc contacts is in agreement with the proposed arrangement of GPs

484   on the surface of PUUV and TULV particles, consisting of Gn-Gc hetero-octamers (i.e. four

485   Gn and four Gc) interconnected via a small Gc:Gc interaction patch (18, 20, 38). By using

486   mutations that stabilize (H303C) or destabilize (H303E) the Gc:Gc contact region between

487   spikes on viral particles (23), we observed by N&B that the Gc-Gc interactions that occur in

488   the GA of living cells are directed by the same contact interface in absence of Gn. The H303C

489   Gc substitution induced dimers very efficiently while, conversely, the H303E substitution

490   hindered dimer formation (Fig. 3). We were thus able to discern subtle changes in the apparent

491   monomer-dimer equilibrium directly in living cells and validated previous results that identified

492   specific amino acids at the Gc:Gc inter-spike contact interface as sensitive mediators of this

493   interaction. The Gc:Gc contact surface might be too small to allow the formation of stable Gc

494   dimers in solution, according to the observation that soluble Gc ectodomain remains monomeric

495   in solution (22, 39). However, our results suggest that the confinement of Gc in a two-

496   dimensional geometry within lipid membranes in the GA (and the consequent high local protein

497   concentration) are sufficient to allow Gc:Gc association in living cells. These interactions might

498   be further favored by inter-spike restrains during viral assembly and on the viral surface.

499   Similarly, we also analyzed regions in Gn which are responsible for its quaternary structure.

500   We tested the concentration-dependent multimerization of the mutant ΔGn in which the N-

501   terminal, membrane distal lobes of Gn (21) were deleted (while maintaining the Gn central

502   stalk, transmembrane domain and endodomain). The fact that this Gn mutant also showed

18

503 increasing multimerization from monomers to tetramers – correlating to the local protein

504 concentration (Fig. 4) – suggests that the membrane-distal lobe of Gn is not needed for Gn

505 multimerization. The ca. 4-fold higher concentrations that were required for a significant

506 multimerization to occur indicate that the membrane-distal lobe might contribute to the tetramer

507 stabilization. The lower stability of ΔGn tetramers might also be partially caused by the N-

508 terminal fusion FPs which, despite the 14 amino acid long linker region, may produce partial

509 hindrance at the tetrameric center of the ectodomain, making multimerization less efficient. We

510 previously observed an analogous behavior also for the Influenza A GP hemagglutinin, whose

511 TMD can multimerize although only to a limited extent, compared to the wild-type (30).

Multimerization-concentration curves

513 In previous investigations from our laboratory, we have discussed the possibility of Gn

514 tetramerization in cell models exclusively expressing this viral GP (16). Nevertheless, in that

515 case, only average multimerization values could be obtained and the presence of tetramers had

516 to be assumed *a priori* in order to estimate the amounts of the different oligomeric species. In

517 this extended investigation instead, we have explored a wide range of concentrations and

518 quantified GP multimerization with single-cell resolution. Further, the observation that the

519 apparent multimeric state of Gn saturates at a value of ~4 (Fig. 1 B) proves that Gn tetramers

520 are indeed present (being the predominant multimeric species at concentrations higher than ca.

521 2000 proteins /μm³) and the amount of larger complexes is negligible at all concentrations. A

522 similar conclusion can be drawn about Gc multimerization approaching asymptotically a value

523 of ~2, indicating the presence of a monomer-dimer equilibrium, without the need for *a priori*

524 assumptions deriving from biochemical/structural data.

GP multimerization is consistent for different viral strains and cellular environments

526 Comparison of different HV strains suggests only minor differences in behavior between PUUV

527 and HTNV GPs expressed in CHO-K1 cells (Fig. 2). This is in agreement with the previous

528 observation that, despite the genetic and geographical distinction between strains, the molecular

529 structure of HV GPs are highly conserved (21, 22, 38-40). More in detail, while Gn localizes in

530 the ER for both strains, Gc showed a partial enrichment in the GA for PUUV but not for HTNV,

531 in agreement with a previous report (14). In this context, it is worth noting that former

532 investigations provided conflicting results regarding the intracellular localization of singularly

533 expressed Gn and Gc (12-14). Here, we report a consistent multimerization behavior for both

534 Gn and Gc, when expressed alone, not correlating with their intracellular localization or cell

535 type. For example, we observed that Gc is found in monomeric or dimeric form, independently

536 from viral strain and localization in GA/ER (Fig. 2, S3).

**Gn-Gc large scale hetero-interactions in the GA**

538 While the investigation of singularly expressed GPs can already provide information about the

539 formation of homotypic complexes, it must be noted that HV assembly in physiological

540 conditions occurs exclusively in the presence of both Gn and Gc. The last part of our study

541 deals therefore with the quantification of protein-protein interactions occurring in the presence

542 of both GPs. In detail, it was shown for HTNV (13, 14), PUUV (16), ANDV and SNV (15, 17)

543 that Gn and Gc expressed together (from a single GPC, separate cDNAs or in the context of

544 infection) co-localize in the GA. However, in this study, we quantify for the first time the

545 oligomerization states of each protein in connection to its subcellular localization, its

546 concentration and the concentration of its interaction partner. First, we confirmed that both

547 PUUV Gn and Gc tagged with FPs are enriched in the GA. In this case, though, Gn does not

548 form large oligomers and shows even decreased multimerization extent than when expressed

549 alone (Fig. 5 E). We believe that the decreased oligomerization capabilities of Gn in this case

550 are probably due to the steric hindrance generated by the fluorescent tag present on Gc N-

551 terminus, since SP-mEGFP-Gn alone can readily form tetramers. This result, while originating

552 from a drawback commonly encountered in fluorescence microscopy investigations, has some

553 general implications. First, this is a strong indication of a direct Gn-Gc interaction, since a part

554 of the Gc fluorescent construct appears to interfere with Gn-Gn contacts. Second, the formation

555 of even relatively small Gn-Gc hetero-oligomers (Gn remaining monomeric or dimeric in

556 average) seems sufficient for Gn transport to the GA. Third, it demonstrates that Gn-Gc

557 interactions do not require the previous formation of Gn homo-tetramers (in disagreement with

558 assembly model 1 proposed by Hepojoki et al. (24)).

559 The possibility that Gn-Gc multimerization is hindered when both GPs contain a fluorescent

560 label is confirmed by the observation that, in the presence of unlabeled Gc, Gn forms multimers

561 with up to eight subunits in average. We therefore developed a novel quantitative fluorescence

562 approach to monitor the interactions between a fluorescent protein and an unlabeled protein,

563 while also being able to estimate the concentrations of both interacting partners (see Figs. 5 E

564 and 6). Using this approach, we observed that, in the presence of non-fluorescent Gc, Gn forms

565 large oligomers, containing up to 8-12 subunits. It must be noted that, in contrast to the case of

566 singularly expressed Gn, we did not observe saturation of Gn multimerization even for the

567 highest concentrations considered. This suggests that even larger Gn multimers might be

20

568   present in this samples and the observed multimerization is in fact an average estimate. Also,

569   the weak correlation between Gn multimerization and Gc concentration (Fig. S8) indicates that

570   the formation of larger Gn complexes does not require preformed Gc:Gc dimeric association

571   (that occurs at high Gc concentrations, see Fig. 1 D). Instead, the results support the idea that

572   Gn and Gc may associate already at low concentrations, subsequently allowing the formation

573   of higher order Gn-Gc species.

574   For the case of Gc in the presence of (non-fluorescent) Gn, instead, the apparent

575   multimerization ranges between two and four, in average (i.e. oligomers with more than four

576   units might also be present, albeit in small amounts). Since only Gc dimers are observed at best

577   in the absence of Gn, multimers containing more than two Gc units must be mediated by Gn

578   oligomers. The same holds true for Gn tetramers as largest Gn oligomer in the absence of Gc

579   (i.e. four Gn units). The observation of Gc complexes with approximately four units diffusing

580   as a whole might be explained by several Gn-Gc configurations, such as those shown in Fig. 7

581   A-D.

582

583
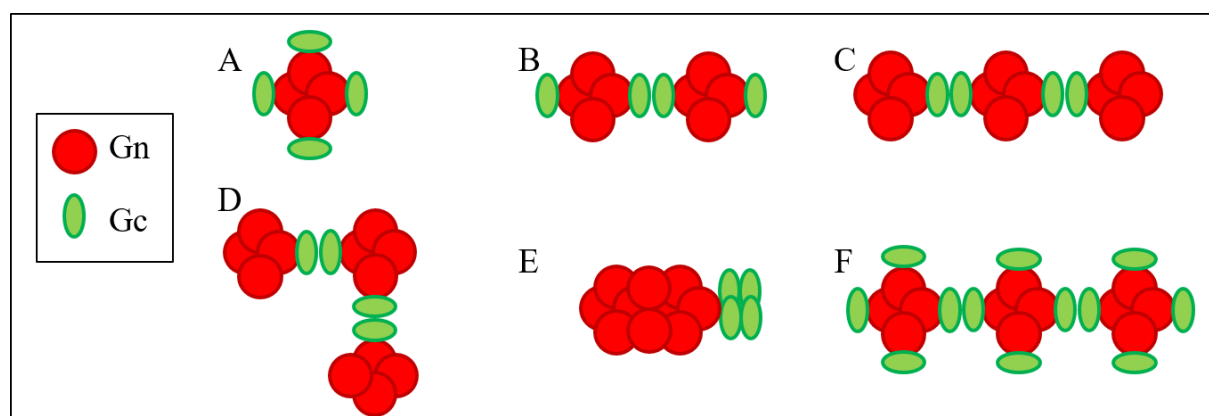
584   **Figure 7: Examples of Gn-Gc hetero-multimers compatible and incompatible with the highest observed**

585   **multimerization states in cells expressing both Gn and Gc.** A-D) Examples of hetero-multimers containing 4

586   Gc units and 4-12 Gn units. E) Gn-Gc arrangement containing a Gn homo-decamer linked to a Gc tetramer. Such

587   hetero-multimer is compatible with the results shown in Figs. 5 and 6, but not with the GP quaternary structure

588   observed for Gn (or Gc) in the absence of the other GP (Fig. 1). F) Gn-Gc hetero-octamers connected via Gc:Gc

589   contacts described for the surface of viral particles (21, 23).

590

591   Larger Gn-Gc hetero-multimers, such as those described in Fig. 7 B-D, are additionally in line

592   with the observation of high multimeric states for Gn mentioned before. Also, alternative spatial

593   arrangements of Gn-Gc hetero-multimers (see e.g. the large Gn homo-multimer linked to a Gc

21

594   homo-tetramers in Fig. 7 E) would not be compatible with the largest Gn (or Gc) homo-
595   oligomers observed in the absence of the other GP, i.e. tetramers (or dimers).

596   Clearly, we cannot exclude that the limited degree of Gc oligomerization (i.e. the limited
597   amount of Gc monomers participating in the described possible Gn-Gc hetero-multimers) might
598   be partially due to the presence of the N-terminal fluorescent tags. Our experiments cannot rule
599   out the possibility that, in the absence of FPs, more Gc monomers might be present in Gn-Gc
600   hetero-multimers (see e.g. Fig. 7 F). It is important to stress therefore that the FPs might have
601   prevented a Gn-Gc stoichiometry of 1:1 that is otherwise guaranteed in natural infections.
602   Nevertheless, it must be noted these results validate in general the proposed GP organization
603   on the viral surface as Gn tetramers connected via Gc:Gc contacts (21, 23, 24). Finally, the lack
604   of correlation between Gc multimerization and Gn concentration suggests once more that the
605   assembly model 1 (24) cannot be entirely accurate, since that would require the formation of
606   Gn multimers (i.e. higher Gn concentrations) for Gc multimerization to occur.

607   **Conclusions**

608   We have investigated the multimerization of HV envelope protein Gn and Gc from "old-world"
609   HV, both singularly or expressed together in living cells, using quantitative fluorescence
610   microscopy approaches. Based on our findings, we can validate a spike assembly model (based
611   on the assembly model 2 proposed by Hepojoki et al. (24)) according to which Gn-Gc small
612   hetero-oligomers (formed e.g. by a Gn dimer and a Gc monomer or, simply, a Gn-Gc hetero-
613   dimer) are first formed in the ER allowing translocation of this complex to the GA. There, Gn-
614   Gn interactions drive the formation of the hetero-octameric complex and Gc stabilizes contacts
615   between neighboring spikes. The further assembly into still larger complexes is reasonably
616   hindered by the presence of FPs in this case. While the presented method appears thus
617   inherently limited by the influence of the fluorescent labels, it is worth stressing that we provide
618   here, for the first time, direct evidence for the initial steps of HV assembly in the GA of living
619   cells. The non-disruptive method presented in this work opens therefore the possibility for
620   further investigations in the context of HV assembly, including for example the characterization
621   of the interaction between GPs and the ribonucleocapsid protein (RNP) or other viral
622   components.

623

624

625

Acknowledgements

Contributions

Research planning, N.D.T. and S.C.; investigation, R.A.P. and A.A.K.; data analysis, R.A.P. and A.A.K.; writing–original draft preparation, R.A.P. and S.C.; writing–review and editing, A.A.K. and N.T.; software, R.A.P.; supervision, S.C.; funding acquisition, N.D.T. and S.C.

References

1. **Ermonval M, Baychelier F, Tordo N.** 2016. What Do We Know about How Hantaviruses Interact with Their Different Hosts? Viruses **8**.

2. **Hjelle B, Torres-Perez F.** 2010. Hantaviruses in the americas and their role as emerging pathogens. Viruses **2:**2559-2586.

3. **Schmaljohn C, Hjelle B.** 1997. Hantaviruses: a global disease problem. Emerg Infect Dis **3:**95-104.

4. **Garoff H, Hewson R, Opstelten DJ.** 1998. Virus maturation by budding. Microbiol Mol Biol Rev **62:**1171-1190.

5. **Lyles DS.** 2013. Assembly and budding of negative-strand RNA viruses. Adv Virus Res **85:**57-90.

6. **Pettersson RF, Melin L.** 1996. Synthesis, assembly, and intracellular transport of Bunyaviridae membrane proteins, p 159-188, The Viruses, The Bunyaviridae. Springer, Boston, MA.

7. **Lober C, Anheier B, Lindow S, Klenk HD, Feldmann H.** 2001. The Hantaan virus glycoprotein precursor is cleaved at the conserved pentapeptide WAASA. Virology **289:**224-229.

8. **Cifuentes-Munoz N, Salazar-Quiroz N, Tischler ND.** 2014. Hantavirus Gn and Gc envelope glycoproteins: key structural units for virus cell entry and virus assembly. Viruses **6:**1801-1822.

9. **Hepojoki J, Strandin T, Lankinen H, Vaheri A.** 2012. Hantavirus structure-- molecular interactions behind the scene. J Gen Virol **93:**1631-1644.

10. **Matsuoka Y, Chen SY, Holland CE, Compans RW.** 1996. Molecular determinants of Golgi retention in the Punta Toro virus G1 protein. Arch Biochem Biophys **336:**184-189.

11. **Andersson AM, Melin L, Persson R, Raschperger E, Wikstrom L, Pettersson RF.** 1997. Processing and membrane topology of the spike proteins G1 and G2 of Uukuniemi virus. J Virol **71:**218-225.

12. **Pensiero MN, Hay J.** 1992. The Hantaan virus M-segment glycoproteins G1 and G2 can be expressed independently. J Virol **66:**1907-1914.

13. **Ruusala A, Persson R, Schmaljohn CS, Pettersson RF.** 1992. Coexpression of the membrane glycoproteins G1 and G2 of Hantaan virus is required for targeting to the Golgi complex. Virology **186:**53-64.

668   14.   **Shi X, Elliott RM.** 2002. Golgi localization of Hantaan virus glycoproteins requires
669   coexpression of G1 and G2. Virology **300:**31-38.

670   15.   **Spiropoulou CF, Goldsmith CS, Shoemaker TR, Peters CJ, Compans RW.** 2003.
671   Sin Nombre virus glycoprotein trafficking. Virology **308:**48-63.

672   16.   **Sperber HS, Welke RW, Petazzi RA, Bergmann R, Schade M, Shai Y, Chiantia**
673   **S, Herrmann A, Schwarzer R.** 2019. Self-association and subcellular localization of
674   Puumala hantavirus envelope proteins. Sci Rep **9:**707.

675   17.   **Deyde VM, Rizvanov AA, Chase J, Otteson EW, St Jeor SC.** 2005. Interactions
676   and trafficking of Andes and Sin Nombre Hantavirus glycoproteins G1 and G2.
677   Virology **331:**307-315.

678   18.   **Huiskonen JT, Hepojoki J, Laurinmaki P, Vaheri A, Lankinen H, Butcher SJ,**
679   **Grunewald K.** 2010. Electron cryotomography of Tula hantavirus suggests a unique
680   assembly paradigm for enveloped viruses. J Virol **84:**4889-4897.

681   19.   **Battisti AJ, Chu YK, Chipman PR, Kaufmann B, Jonsson CB, Rossmann MG.**
682   2011. Structural studies of Hantaan virus. J Virol **85:**835-841.

683   20.   **Hepojoki J, Strandin T, Vaheri A, Lankinen H.** 2010. Interactions and
684   oligomerization of hantavirus glycoproteins. J Virol **84:**227-242.

685   21.   **Li S, Rissanen I, Zeltina A, Hepojoki J, Raghwani J, Harlos K, Pybus OG,**
686   **Huiskonen JT, Bowden TA.** 2016. A Molecular-Level Account of the Antigenic
687   Hantaviral Surface. Cell Rep **16:**278.

688   22.   **Guardado-Calvo P, Bignon EA, Stettner E, Jeffers SA, Perez-Vargas J, Pehau-**
689   **Arnaudet G, Tortorici MA, Jestin JL, England P, Tischler ND, Rey FA.** 2016.
690   Mechanistic Insight into Bunyavirus-Induced Membrane Fusion from Structure-
691   Function Analyses of the Hantavirus Envelope Glycoprotein Gc. PLoS Pathog
692   **12:**e1005813.

693   23.   **Bignon EA, Albornoz A, Guardado-Calvo P, Rey FA, Tischler ND.** 2019.
694   Molecular organization and dynamics of the fusion protein Gc at the hantavirus
695   surface. Elife **8**.

696   24.   **Hepojoki J, Strandin T, Wang H, Vapalahti O, Vaheri A, Lankinen H.** 2010.
697   Cytoplasmic tails of hantavirus glycoproteins interact with the nucleocapsid protein. J
698   Gen Virol **91:**2341-2350.

699   25.   **Zacharias DA, Violin JD, Newton AC, Tsien RY.** 2002. Partitioning of lipid-
700   modified monomeric GFPs into membrane microdomains of live cells. Science
701   **296:**913-916.

702   26.   **Chen X, Zaro JL, Shen WC.** 2013. Fusion protein linkers: property, design and
703   functionality. Adv Drug Deliv Rev **65:**1357-1369.

704   27.   **Bird RE, Hardman KD, Jacobson JW, Johnson S, Kaufman BM, Lee SM, Lee T,**
705   **Pope SH, Riordan GS, Whitlow M.** 1988. Single-chain antigen-binding proteins.
706   Science **242:**423-426.

707   28.   **Orekhova AS, Sverdlova PS, Spirin PV, Leonova OG, Popenko VI, Prasolov VS,**
708   **Rubtsov PM.** 2011. [Novel bidirectional promoter from human genome]. Mol Biol
709   (Mosk) **45:**486-495.

710   29.   **Chiantia S, Ries J, Schwille P.** 2009. Fluorescence correlation spectroscopy in
711   membrane structure elucidation. Biochim Biophys Acta **1788:**225-233.

712   30.   **Dunsing V, Luckner M, Zuhlke B, Petazzi RA, Herrmann A, Chiantia S.** 2018.
713   Optimal fluorescent protein tags for quantifying protein oligomerization in living cells.
714   Sci Rep **8:**10634.

715   31.   **Dunsing V, Chiantia S.** 2018. A Fluorescence Fluctuation Spectroscopy Assay of
716   Protein-Protein Interactions at Cell-Cell Contacts. J Vis Exp doi:10.3791/58582.

717   32.   **Digman MA, Dalal R, Horwitz AF, Gratton E.** 2008. Mapping the number of
718   molecules and brightness in the laser scanning microscope. Biophys J **94:**2320-2332.

719   33.   **Dunsing V, Mayer M, Liebsch F, Multhaup G, Chiantia S.** 2017. Direct evidence
720   of amyloid precursor-like protein 1 trans interactions in cell-cell adhesion platforms
721   investigated via fluorescence fluctuation spectroscopy. Mol Biol Cell **28:**3609-3620.

722   34.   **Spiropoulou CF.** 2013. Hantavirus maturation, p 33-44, Hantaviruses. Springer
723   Science & Business Media.

724   35.   **Bobone S, Hilsch M, Storm J, Dunsing V, Herrmann A, Chiantia S.** 2017.
725   Phosphatidylserine Lateral Organization Influences the Interaction of Influenza Virus
726   Matrix Protein 1 with Lipid Membranes. J Virol **91**.

727   36.   **Chen Y, Johnson J, Macdonald P, Wu B, Mueller JD.** 2010. Observing protein
728   interactions and their stoichiometry in living cells by brightness analysis of
729   fluorescence fluctuation experiments. Methods Enzymol **472:**345-363.

730   37.   **Macdonald P, Johnson J, Smith E, Chen Y, Mueller JD.** 2013. Brightness analysis.
731   Methods Enzymol **518:**71-98.

732   38.   **Rissanen I, Stass R, Zeltina A, Li S, Hepojoki J, Harlos K, Gilbert RJC,**
733   **Huiskonen JT, Bowden TA.** 2017. Structural Transitions of the Conserved and
734   Metastable Hantaviral Glycoprotein Envelope. J Virol **91**.

735   39.   **Willensky S, Bar-Rogovsky H, Bignon EA, Tischler ND, Modis Y, Dessau M.**

736   2016. Crystal Structure of Glycoprotein C from a Hantavirus in the Post-fusion

737   Conformation. PLoS Pathog **12:**e1005948.

738   40.   **Guardado-Calvo P, Rey FA.** 2017. The Envelope Proteins of the Bunyavirales. Adv

739   Virus Res **98:**83-118.

740